Journal of Materials Chemistry C

PAPER

View Article Online
View Journal | View Issue



Cite this: J. Mater. Chem. C, 2018, 6, 2295

# Perovskite templating *via* a bathophenanthroline additive for efficient light-emitting devices†

Nur Fadilah Jamaludin,‡[abc] Natalia Yantara,‡[a] Yan Fong Ng,[abc] Annalisa Bruno,[a] Bevita K. Chandran,[abc] Xin Yu Chin,[a] Krishnamoorthy Thirumal,[a] Nripan Mathews,[ac] Cesare Soci[d] and Subodh Mhaisalkar*[ac]

Received 9th December 2017,
Accepted 1st February 2018

DOI: 10.1039/c7tc05643e

rsc.li/materials-c

Identified as emerging light absorbers due to their plethora of unique optoelectronic properties, perovskites have also been touted as a promising candidate for light emission. However, despite the effortless transition of perovskites into the current organic light-emitting diodes (OLEDs), misalignment of energy levels at the hole transporting material (HTM) and perovskite interface limits the efficacy of interfacial charge transport. Herein, it is shown that by incorporating a small organic molecule, bathophenanthroline (BPhen), into the $CH_3NH_3PbBr_3$ emitter *via* a solvent engineering technique, the energy band levels of the perovskite can be tailored and the energy mismatch at the HTM/perovskite interface can be ameliorated through the formation of a graded emitter layer and accompanying morphological improvements. With a BPhen concentration of 0.500 mg $mL^{-1}$, more than ten-fold enhancement of device luminance and efficiency was achieved, thus demonstrating a facile and viable approach for fabricating high-performance perovskite light-emitting diodes (PeLEDs).

## Introduction

Offering a wide array of excellent optoelectronic properties such as direct band gap, high extinction coefficient and low defect density,[1–3] organic–inorganic hybrid halide perovskites have shown tremendous success as light absorbers in recent years. The similar properties required for both light-harvesting and -emitting applications indicate the potential of perovskites beyond the field of photovoltaics.[4] This, coupled with early reports of narrow photoluminescence (PL) emission bands[5,6] observed in perovskites, has driven research into the employment of these materials in light-emitting diodes (PeLEDs),[4,7] with the current state-of-the-art devices boasting the external quantum efficiency (EQE) values beyond 10%.[8,9]

The expeditious rise in PeLED performance can be ascribed to the compatability of perovskites with OLED device architecture[10–12] which facilitates the technological transfer. In addition, the low material and processing costs of perovskites[2,13,14] further fortify efforts to realize a cheap and viable alternative to current OLEDs. Recent improvements in PeLED device performance have been dominated by process-engineered grain size modulation techniques to improve film morphology, such as nanocrystal pinning,[15] and use of polymer composites,[16,17] all in a bid to increase radiative recombination through spatial confinement of injected charges. However, an equally important aspect that is often overlooked is the energy band alignment across the material stack. Energy mismatch culminates in charge build-up at the heterojunctions between the perovskite emitter and the charge selective layers. These discrete interfaces are detrimental to the overall device performance owing to two main reasons: (i) a high energetic barrier for charge injection which consequently leads to (ii) a high electric field across the interface thereby possibly exacerbating Joule heating effects.[18]

Reports from OLED studies have shown that the effect of an abrupt change in interfacial energy levels can be mitigated through the employment of a graded device architecture.[18,19] Lee and co-workers have previously reported the use of a buffered hole injection layer using perfluorinated ionomers (PFI) to increase the work function of PEDOT:PSS and reduce the hole injection energy barrier across the HTM/perovskite interface, resulting in improved performances of their PeLED devices.[15,20] However, it has been revealed that PFI-modified HTM yields larger contact resistance and lower equilibrium

[a] Energy Research Institute @ NTU (ERI@N), Nanyang Technological University, Research Techno Plaza, X-Frontier Block, Level 5, 50 Nanyang Drive, 637553, Singapore. E-mail: subodh@ntu.edu.sg
[b] Interdisciplinary Graduate School, Nanyang Technological University, 50 Nanyang Avenue, 639798, Singapore
[c] School of Materials Science and Engineering, Nanyang Technological University, 50 Nanyang Avenue, 639798, Singapore
[d] Division of Physics and Applied Physics, School of Physical and Mathematical Sciences, Nanyang Technological University, 21 Nanyang Link, 637371, Singapore

† Electronic supplementary information (ESI) available: FTIR, PL spectra, Elliot fitting of absorbance spectra, and statistics on device performance. See DOI: 10.1039/c7tc05643e

‡ These authors contributed equally to this work.

density of holes at the interfacial contact as a result of lower interfacial capacitance and loss of polaron stabilization energy.[21] Thus, even if the higher work function matches the valence band of the perovskite, the interfacial contact remains non-ohmic and the high carrier density desired at the interface cannot be achieved. A different approach is then required to modulate and refine the energy band alignment.

One way of doing so is through the implementation of a graded emitter layer to better match the interfacial charge selective layers. In this case, instead of modifying the HTM, a graded emitter energy band is obtained through the incorporation of an electron transporting organic molecule, bathophenanthroline (BPhen), into the perovskite. Typically for OLEDs, charge imbalance occurs due to the lower electron mobility in the electron transporting material (ETM) as compared to holes in the HTM. To circumvent the translation of this problem for PeLEDs due to the adoption of a similar OLED device architecture, BPhen, offering high electron mobility, was chosen. While it is expected that energy level modulation would occur at the perovskite/ETM interface, it is fascinating to note that the same trend was also observed for the HTM/perovskite interface. The key to control the shift in energy levels is through variation of BPhen concentration in the anti-solvent. By simply dissolving BPhen in toluene and subsequently dripping it onto the substrate midway during spin coating *via* a process known as solvent engineering, the small phenanthroline molecule is integrated into the perovskite. The perovskite energy band moves upwards upon increasing BPhen concentration, resulting in the minimization of an injection barrier at the HTM/perovskite interface, thereby facilitating hole injection into the emitter. This is in strong agreement with the published literature which has also shown that incorporation of additives into perovskite's anti-solvent can influence perovskite's work function and energy level alignments to form a graded structure.[22–25] The simultaneous grain size reduction and the resulting spatial charge confinement further facilitate radiative recombination translating to a multi-fold improvement in performance as compared to the reference $CH_3NH_3PbBr_3$ devices.

# Experimental section

### Material synthesis

The films characterized in this study were prepared as follows: $CH_3NH_3PbBr_3$ solution was prepared with a 1 : 1.05 molar ratio of $PbBr_2$ (TCI) and $CH_3NH_3Br$ (Dyesol) in a co-solvent of DMF and DMSO (3 : 1) to form a solution of 1 M concentration. The reference film was spin coated at 5000 rpm for 12 s with an anti-solvent (toluene), introduced 4 s from the initiation of the spin coating process to facilitate rapid crystallization. The small molecule additive was incorporated into the perovskite layer by first dissolving Bathophenanthroline (BPhen) (Aldrich, 97%) in toluene prior to use as an anti-solvent during the spin coating process. BPhen concentration ranging from 0 to 0.750 mg $mL^{-1}$ in toluene was utilized throughout the experiment. The films were thereafter allowed to dry under vacuum for 30 min.

### Device fabrication

The devices, on the other hand, were fabricated on indium-doped tin oxide (ITO, 7 $\Omega$ $sq^{-1}$) coated glass substrates. The substrates were first cleaned successively using soap, deionized water and ethanol before being dried and plasma cleaned for 15 min. PEDOT:PSS (Clevios P VP Al4083) was then spin coated at 4000 rpm for 60 s and annealed at 130 °C for 15 min to remove excess moisture. The BPhen-incorporated films were then spin coated and vacuum dried, prior to evaporation of the electron transporting layer (ETL) and cathode. 2,4,6-Tris[3-(diphenylphosphinyl)phenyl]-1,3,5-triazine (PO-T2T) (Lumtec, >99%) (45 nm), calcium (Ca) and aluminium (Al) were thermally evaporated to form the ETL and cathode respectively. Evaporation was done under vacuum ($<1 \times 10^{-6}$ Torr) and encapsulated with UV curing epoxy prior to testing. The measured device area is 8 $mm^2$.

### Material characterization

Valence band maximum estimations were carried out using a Riken Keiki AC-2 spectrometer with a power setting and power number of 856.8 nW and 0.5 respectively. All phase and composition analysis of the prepared films were characterized using a Shimadzu XRD-6000 with a $2\theta$ scan mode (fixed $\theta$) and scintillation counter detector. Measurements were carried out for the range of 10–60° using a Cu K$\alpha$ X-ray tube ($\lambda$ = 1.54 Å). A UV-VIS-NIR spectrophotometer (Shimadzu UV-3600) was used to obtain the absorption spectra of the $CH_3NH_3PbBr_3$ thin films with an integrating sphere attachment (ISR-3100). All the steady-state photoluminescence measurements were taken using a Fluoromax-4 (Horiba Jobin Yvon) spectrofluorometer with an excitation wavelength of 400 nm and the intensities were corrected against the absorbance for the same excitation wavelength. All the time-resolved photoluminescence measurements were obtained using a Picoquant PicoHarp 300 time-correlated single photon counting (TCSPC) system coupled to a micro-PL setup with a Nikon microscope objective (20× magnification, NA = 0.3). A ps-pulsed laser diode ($\lambda$ = 405 nm, $f$ = 40 MHz) (Picoquant P-C-405B) was used to excite the sample. The output signal is then fibre coupled to Acton SP-2300i monochromator (300 mm focal length) for spectral selection of the emission light at 540 nm with a slit width of 15 nm. Another optical fibre connected to the output of the monochromator is used to couple spectral separated output light to an avalanche diode that is synchronized with the excitation laser *via* the TCSPC electronic. Overall, the FWHM of the system instrument respond function is expected to be at 50 ps. The FTIR measurements were done under vacuum (2–5 mbar) with BPhen-incorporated films prepared on $CaF_2$ substrates, using a GLOBAR lamp with KBr and liquid-nitrogen cooled MCT (mercury–cadmium–telluride) used as the beam splitter and detector respectively. The instrument detection limit is 0.0001. All the topological and potential mapping images were obtained using the tapping and Kelvin Probe Force Microscope (KPFM) modes of the Asylum Research MFP-3D AFM. Ti/Ir coated cantilevers (ASYELEC-01-R2, Asylum Research) with a spring constant and resonance frequency of 2.8 N $m^{-1}$ and 78 kHz were used for the measurements.

 

Morphological characterization was done using a JEOL 7600F with a field emission electron source offering a resolution of 1.5 nm. The accelerating voltage was kept at 5 keV during the imaging process.

### Device characterization

All device testing was done outside the glovebox under ambient conditions. The device characteristics (*J–V–L*) and electroluminescence spectra were collected with a Keithley 2612B source meter and an OceanOptics QE Pro spectrometer with an attached integrating sphere.

## Results and discussion

As previously mentioned, the films used in this study were prepared using the widely reported solvent engineering process, which allows for the facile fabrication of smooth and compact perovskite films. By tuning the BPhen concentration in the anti-solvent from 0 to 0.750 mg $mL^{-1}$, notable enhancement to the films' optoelectronic properties and device performance were observed. To ascertain the films' phase purity on BPhen incorporation, compositional evaluation using X-Ray Diffraction (XRD) was carried out. Fig. 1a shows the XRD patterns of the $CH_3NH_3PbBr_3$ films prepared with varying BPhen concentration. Analysis of the patterns revealed characteristic reflections of the $CH_3NH_3PbBr_3$ cubic (*Pm*3*m*) phase,[26–28] with no extra peaks to imply the presence of secondary phases. Intriguingly, inclusion of BPhen resulted in more crystalline films (as inferred by the sharpening of the XRD peaks), consisting of crystallites with a reduced tendency for preferred orientation (indicated by the presence of additional XRD peaks corresponding to orientations other than the (001) plane). Negligible changes in the lattice parameters were also observed, concurring with the report by Cho *et al.*, where inclusion of a small molecule additive induced no change to the perovskite crystal structure.[15] The incorporation

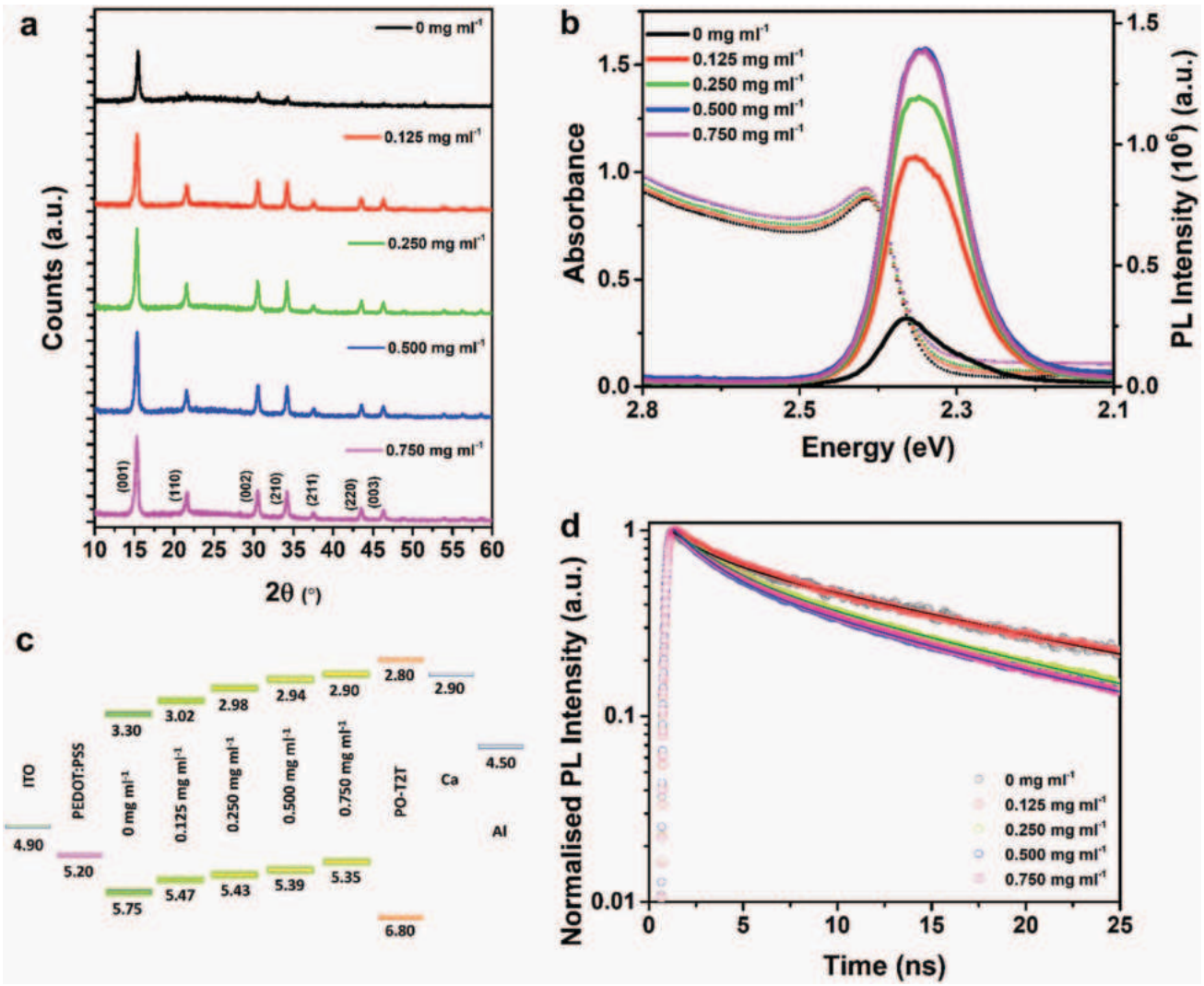


Fig. 1 (a) XRD pattern, (b) absorbance and absorbance corrected photoluminescence spectra, (c) energy band levels and (d) time-resolved photoluminescence decays of BPhen-incorporated $CH_3NH_3PbBr_3$ films with various concentrations ranging from 0 to 0.750 mg $mL^{-1}$. Units for energy levels are in eV.

of BPhen in perovskite *via* the templating process was confirmed using Fourier transform infrared spectroscopy (FTIR) (Fig. S1, ESI†).

Based on the premise that a highly photoluminescent material is well suited for light emission applications,[4] the influence of BPhen concentration on PL intensity was investigated. Fig. 1b shows the absorbance and PL emission spectra (absorbance-corrected) of the reference and BPhen-incorporated films. Here, the absorbance-corrected PL emission spectra are presented to account for re-absorption of emitted photons at the excitation wavelength (400 nm). The optical band gap (~2.40 eV) and exciton binding energy (~50 meV) of the films extracted with Elliot's fitting (Fig. S2 and Table S1, ESI†),[29,30] as well as the corresponding PL peak energy (~2.3 eV), were found to be nearly unaffected by BPhen incorporation. Remarkably, the PL intensity increases substantially with increasing BPhen concentration up to 0.500 mg $mL^{-1}$, beyond which the intensity saturates, implying a strong correlation between BPhen concentration and radiative recombination yield. While double emission peaks were noted in the PL spectra of the reference and BPhen-incorporated films up to 0.250 mg $mL^{-1}$ (Fig. S3, ESI†) due to either the co-existence of ordered and disordered domains[31] or to an inner filtering effect,[32,33] films prepared with higher BPhen concentrations showed only a single PL peak emission. This can be explained by the formation of increasingly ordered domains for the 0.500 and 0.750 mg $mL^{-1}$ Bphen-incorporated films.

The energy band alignments of the films were obtained from photoelectron spectroscopy in air (PESA) (Fig. S4, ESI†) and ultraviolet-visible (UV-vis) absorption measurements. Fig. 1c represents the change in emitter valence and conduction band levels as well as the corresponding optical band gaps as reported in Table S1 (ESI†) on increasing BPhen concentration. The upward shift of the energy levels with higher BPhen concentration suggests that its addition during processing offers interfacial band engineering which can be imputed to the stoichiometric modification[34] or accommodation of the BPhen molecule in the microstructure. This consequently reduces the hole injection barrier through better matching at the HTM/perovskite interface without introducing any additional energy barrier at the electron transporting layer (ETL)/perovskite interface. The reduction in energetic offset between the conduction band of the perovskite and the lowest unoccupied molecular orbital (LUMO) of the ETL is expected to improve electron transfer and reduce energy loss, while the larger offset between the valence band of the perovskite and the highest occupied molecular orbital (HOMO) of the ETL would increase the hole blocking capabilities of this interface.

The effect of BPhen addition in the $CH_3NH_3PbBr_3$ films was also probed through time-resolved PL (TRPL) decay measurements to scrutinize the influence of BPhen inclusion on PL radiative lifetimes. Fig. 1d shows the TRPL decays for the reference and BPhen incorporated films. The decay curves are fitted with a bi-exponential decay function to extract the fast and slow time constants related to the non-radiative and radiative recombination processes occurring in the films. It was found that the weighted average lifetimes decreased with increasing BPhen concentration (Table S2, ESI†). This can be attributed to either an increase in defect states or decrease in film grain size, where an enhanced radiative recombination rate is triggered due to the spatial confinement offered by the latter.[35] It is postulated that grain size reduction is a more plausible explanation for the shortened TRPL decay lifetime owing to the improvement in PL intensities noted with BPhen incorporation (Fig. 1b).

Topological assessment of the films was carried out to verify the hypothesis of grain size modulation on BPhen incorporation. Fig. 2a and b display the top-view and cross-sectional field emission scanning electron microscope (FESEM) images of the reference and BPhen-incorporated films of varying concentrations. Although thickness (*ca.* 400 nm) and surface coverage remain unaffected with increasing BPhen concentration, the grain boundaries become progressively more conspicuous. From the cross-sectional images of the films in Fig. 2b(i–v), a noticeable change from columnar to polycrystalline grain structures was observed with increasing BPhen concentration, although larger surface roughness was also detected (Fig. S5, ESI†). While the reference $CH_3NH_3PbBr_3$ film consists of a single layer of large columnar grains (>200 nm in size), it is curious to note that the BPhen-incorporated films exhibit a

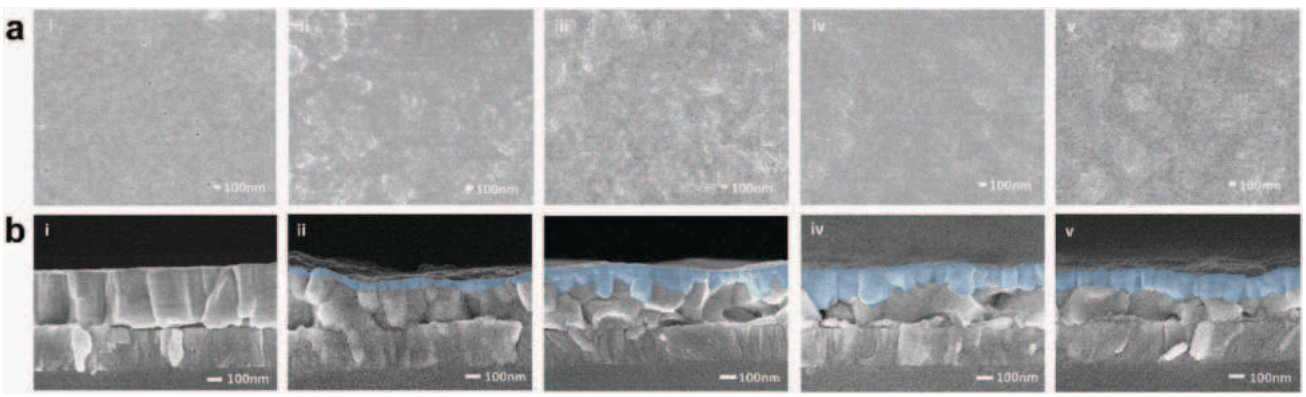


Fig. 2 (a) Top-view (surface) and (b) cross-sectional images of $CH_3NH_3PbBr_3$ films prepared with BPhen concentrations of (i) 0, (ii) 0.125, (iii) 0.250, (iv) 0.500 and (v) 0.750 mg $mL^{-1}$ on ITO/PEDOT:PSS substrates. The smaller grains obtained with BPhen addition are indicated in blue.

bimodal grain size distribution, with the bottom layer consisting of larger grains (>200 nm) and the overlayer consisting of smaller grains (<100 nm). The smaller grains in the overlayer can be ascribed to the pinning effect of the small molecule additive,[15] while the formation of a double layer implies that the pinning effect only occurs at the top surface during the solvent engineering process. Since the smaller grains are known to enhance radiative recombination through stronger spatial charge confinement,[35] we ascribe the higher PL emission reported in Fig. 1b to the presence of the overlayer in BPhen-incorporated films.

BPhen-incorporated PeLEDs were subsequently fabricated to correlate film morphology and optoelectronic properties with device performance. The device characteristics – current density and luminance values as a function of applied voltage, are shown in Fig. 3a. Clearly, the addition of BPhen into the emitter layer improved device performance across all measured parameters. The reference $CH_3NH_3PbBr_3$ device gave a peak luminance of 2000 cd $m^{-2}$ at 8.5 V – inferior to the BPhen-incorporated devices, which exhibited substantially higher luminance (>10 000 cd $m^{-2}$) at much lower voltages. The threshold voltage, indicative of carrier injection efficiency,[36] is reduced to the range 2.3–2.8 V, a notable improvement from the reference (>35 V). Current efficiencies and EQE (Fig. 3b and c) were also well above those of the reference device, consistent with the higher luminance attained for comparable current densities. Our best device was achieved with a BPhen concentration of 0.500 mg $mL^{-1}$, yielding maximum luminance, current efficiency and EQE of 19 627 cd $m^{-2}$, 3.7 cd $A^{-1}$ and 0.78%, respectively. This is equivalent to a ten-fold increase in luminance and fifteen-fold improvement in current efficiency and EQE as compared to the reference device.

The remarkable enhancement across all performance metrics obtained through a simple incorporation of BPhen implies significant losses in the reference device, which can be mainly attributed to optical and electrical losses.[37] Smaller grains achieved through BPhen incorporation in PeLEDs afford effective radiative recombination of charges due to enhanced spatial confinement.[15] This is consistent with the rapid PL decay and high photoluminescence intensity measured in BPhen-incorporated films.[15,16,38,39] The reduction in threshold

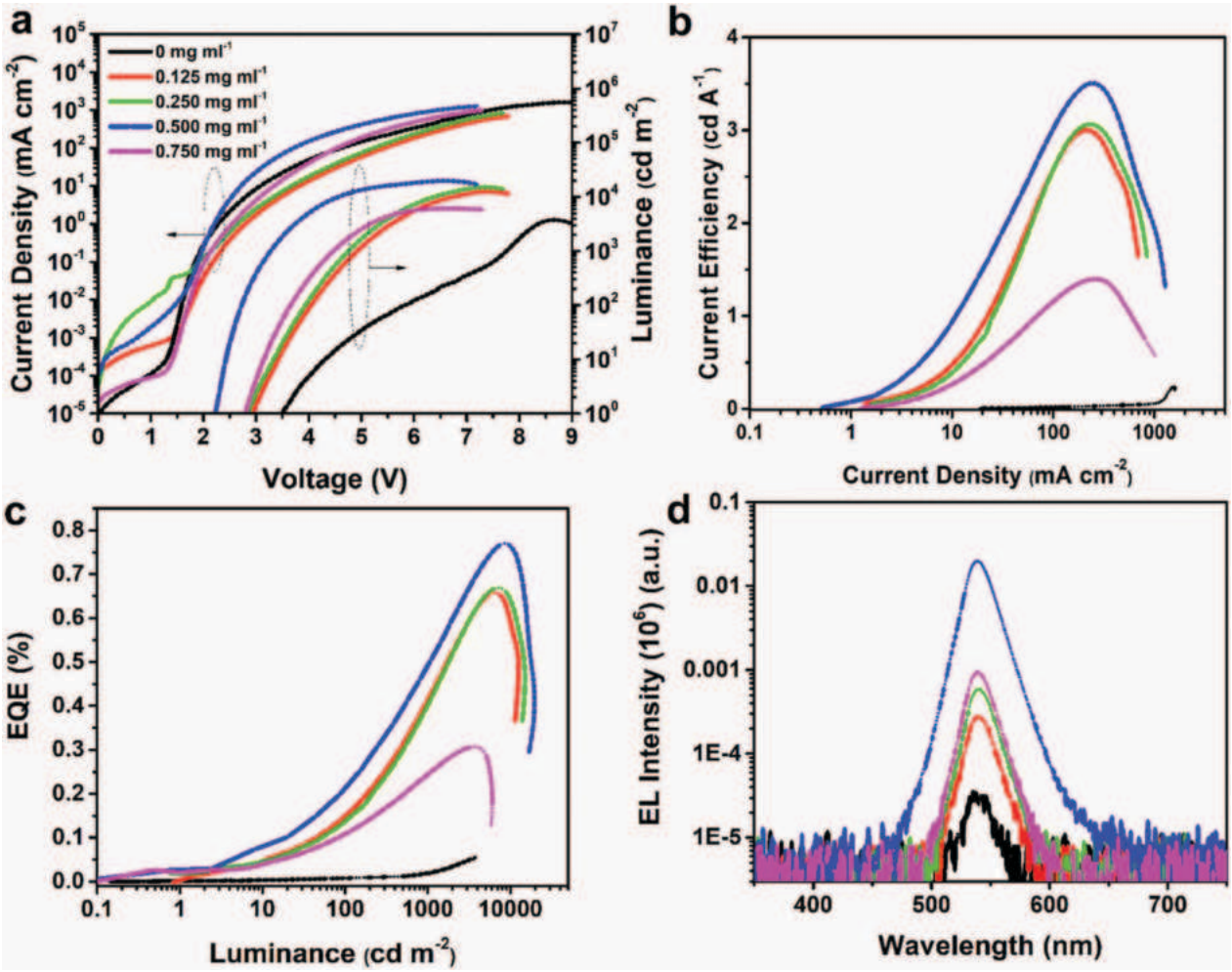


Fig. 3 PeLED characteristics. (a) Current density and luminance against applied voltage, (b) current efficiency against current density, and (c) EQE *versus* luminance curves of reference and BPhen-incorporated $CH_3NH_3PbBr_3$ based devices. (d) Electroluminescence spectra (plotted in semi-logarithmic scale) of tested devices at 4 V bias.

voltage to values as low as the band gap of the emitter implies that the energy barrier at the HTM/perovskite interface is effectively eliminated, due to the re-alignment of energy band levels, facilitating hole injection into the perovskite. Although the energy levels show a continuous shift with higher BPhen concentration ($>0.500$ mg mL$^{-1}$), the decline in device performance can be explained by the need for optimum positioning of the energy levels to facilitate simultaneous carrier injection and confinement. Accordingly, the higher current efficiency recorded also stems from the more effective radiative recombination in BPhen-incorporated devices, giving rise to a higher luminance for similar current densities. In addition, the lone pair of electrons on the sp$^2$-hybridized orbital of N in the pyridine molecules of BPhen could bind with under-coordinated Pb atoms,[40] thus passivating possible trap states (although further studies are needed to verify this hypothesis). The drop in current efficiency upon addition of 0.750 mg mL$^{-1}$ of BPhen, on the other hand, is due to the decrease in carrier mobility arising from increased impurity scattering[41] at high BPhen concentration, as deduced from the lower current density measured in hole-only devices (Fig. S6, ESI†). A comparison of the electroluminescence (EL) spectra of all the devices biased at 4 V is shown in Fig. 3d. The extremely narrow full width at half maximum (*ca.* 20–22 nm) indicates high colour purity emission, as also seen in Fig. S5d (ESI†). Reproducibility of the Bphen incorporated devices was also investigated. Fig. 4 provides a statistical representation of fifty devices for the various performance metrics (maximum luminance, threshold voltage and current efficiency). It is clearly evident that Bphen incorporation offers a consistent advantage across all device parameters compared to the reference. Higher luminance was charted for concentrations ranging from 0.125 to 0.750 mg mL$^{-1}$ which thus reiterates Bphen's role in lowering interfacial injection barrier and facilitating radiative recombination through its incorporation in the emitter layer.

Stability testing was subsequently carried out for the 0 and 0.500 mg mL$^{-1}$ Bphen incorporated films to investigate

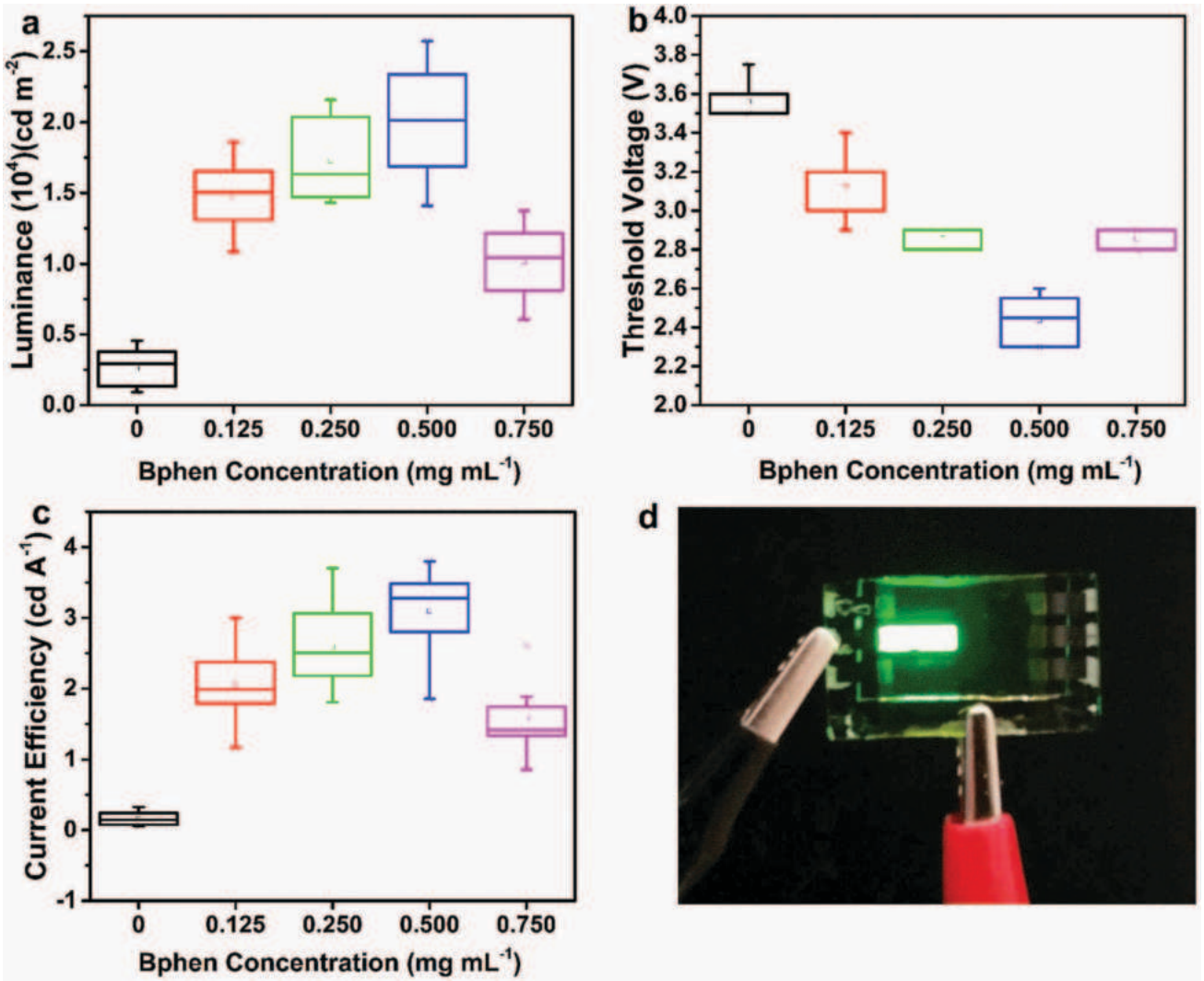


Fig. 4 Statistical representation of the reference and BPhen-incorporated $CH_3NH_3PbBr_3$ devices (up to 10 devices each) in terms of (a) maximum luminance, (b) threshold voltage, and (c) current efficiency. (d) Photographic image of a BPhen-incorporated $CH_3NH_3PbBr_3$ device (area = 8 mm$^2$) under operational condition, showing uniform and colour-pure green emission.

the influence of Bphen incorporation on device performance with time. Prior to constant current measurements, the devices were pre-biased to establish the current density required to illuminate the device to $L_0 \approx 100$ cd $m^{-2}$. The plots of luminance against time for the 0 and 0.500 mg $mL^{-1}$ devices measured under constant current are shown in Fig. S7 (ESI†). It was observed that while the reference (0 mg $mL^{-1}$) device showed a short luminance half-life of approximately 10 s, the 0.500 mg $mL^{-1}$ device persisted fifty times longer. This drastic difference in stability can be simply explained by the higher current density needed for the reference device to achieve comparable luminance levels to the 0.500 mg $mL^{-1}$ device. The two orders of magnitude higher current density required to achieve $L_0 \approx 100$ cd $m^{-2}$ in the reference device (as noted in Fig. 3a) not only enhances the Joule heating effect but also facilitates rapid device degradation.

Finally, two other small organic molecules, namely 1,3,5-tris(1-phenyl-1*H*-benzimidazol-2-yl)benzene (TPBi) and 2-(4-biphenyl)-5-(4-tert-butylphenyl)-1,3,4-oxadiazole (PBD), were also investigated as potential BPhen substitutes because of their deep HOMO levels offering potentially similar hole-blocking capabilities. Fig. S8 (ESI†) provides a comparison of the PL emission spectra of the films incorporated with different molecules with identical concentration. Although TPBi, PBD and BPhen-incorporated $CH_3NH_3PbBr_3$ films gave higher PL emissions, in the respective order, no direct correlation between the PL enhancement and device performance could be found (Fig. S9, ESI†). Rather, BPhen-incorporated devices yielded the best performance, whereas TPBi and PBD-incorporated devices showed similar efficiencies to the reference device. This suggests that the specific choice of small molecule used as the additive plays a crucial role in alleviating the electrical and optical losses of PeLEDs. A few reasons for this are discussed below. First, the electron mobility is highest for BPhen ($5.2 \times 10^{-4}$ $cm^2$ $V^{-1}$ $s^{-1}$), followed by TPBi ($3.3 \times 10^{-5}$ $cm^2$ $V^{-1}$ $s^{-1}$) and PBD ($2 \times 10^{-5}$ $cm^2$ $V^{-1}$ $s^{-1}$), which could have influenced the electron charge dynamics in the perovskite emitter, thus explaining the shift in threshold voltage.[42–44] Second, the size of the organic molecules used will likely determine the extent of incorporation in the perovskite framework. Based on their molecular structure (Fig. S10, ESI†) TPBi and PBD are larger than BPhen, which could distort the perovskite structure and introduce lattice defects. A more thorough investigation of the properties desired for such molecule additives will be conducted in the future, to better design and replicate these findings in other PeLED systems.

## Conclusions

In conclusion, it has been shown that incorporation of BPhen into $CH_3NH_3PbBr_3$ *via* a solvent engineering process leads to improved device performance due to the synergistic effect of smaller grains that improve the yield of radiative recombination and lower electron/hole injection at the ETL/HTM-perovskite interfaces respectively. This is possible thanks to the controllable alteration of the perovskite's energy bands *via* simple variation of the BPhen concentration in the anti-solvent. Our best device was fabricated using 0.500 mg $mL^{-1}$ of BPhen, resulting in a ten-fold increase in luminance and a fifteen-fold improvement in current efficiency and EQE compared to the reference device. Excessive BPhen (>0.500 mg $mL^{-1}$), however, resulted in a decline in device performance, which is attributed to the reduction of charge carrier mobility at high additive concentrations. Although substitution of the small molecule inclusion (BPhen) with PBD and TPBi brings about improvements in PL intensity, the minimal effect seen in device efficiency indicates that the choice of additive molecules requires careful selection so that the resulting film morphology and optoelectronic characteristics have a positive influence on device performance.

## Conflicts of interest

There are no conflicts to declare.

## Acknowledgements

The authors would like to extend their heartfelt gratitude to Mr David Giovanni and Dr Tom Baikie, of Division of Physics and Applied Physics, School of Physical and Mathematical Sciences, Nanyang Technological University and Energy Research Institute @NTU (ERI@N), respectively, for the valuable discussion on excitonic absorption and XRD analysis. The authors would also like to acknowledge the Facility for Analysis, Characterization, Testing and Simulation (FACTS), Nanyang Technological University, Singapore, for the use of their electron microscopy and X-ray facilities. This research was supported by the National Research Foundation, Prime Minister's Office, Singapore under its Competitive Research Programme (CRP Award No. NRF-CRP14-2014-03) and through the Singapore–Berkeley Research Initiative for Sustainable Energy (SinBeRISE) CREATE Program.

## Notes and references

1 P. P. Boix, K. Nonomura, N. Mathews and S. G. Mhaisalkar, *Mater. Today*, 2014, **17**, 16–23.
2 H.-S. Kim, S. H. Im and N.-G. Park, *J. Phys. Chem. C*, 2014, **118**, 5615–5625.
3 S. P. Singh and P. Nagarjuna, *Dalton Trans.*, 2014, **43**, 5247–5251.
4 S. A. Veldhuis, P. P. Boix, N. Yantara, M. Li, T. C. Sum, N. Mathews and S. G. Mhaisalkar, *Adv. Mater.*, 2016, **28**, 6804–6834.
5 Z.-K. Tan, R. S. Moghaddam, M. L. Lai, P. Docampo, R. Higler, F. Deschler, M. Price, A. Sadhanala, L. M. Pazos, D. Credgington, F. Hanusch, T. Bein, H. J. Snaith and R. H. Friend, *Nat. Nanotechnol.*, 2014, **9**, 687–692.
6 N. Yantara, S. Bhaumik, F. Yan, D. Sabba, H. A. Dewi, N. Mathews, P. P. Boix, H. V. Demir and S. Mhaisalkar, *J. Phys. Lett.*, 2015, **6**, 4360–4364.

7 Y.-H. Kim, H. Cho and T.-W. Lee, *Proc. Natl. Acad. Sci. U. S. A.*, 2016, **113**, 11694–11702.
8 N. Wang, L. Cheng, R. Ge, S. Zhang, Y. Miao, W. Zou, C. Yi, Y. Sun, Y. Cao, R. Yang, Y. Wei, Q. Guo, Y. Ke, M. Yu, Y. Jin, Y. Liu, Q. Ding, D. Di, L. Yang, G. Xing, H. Tian, C. Jin, F. Gao, R. H. Friend, J. Wang and W. Huang, *Nat. Photonics*, 2016, **10**, 699–704.
9 Z. Xiao, R. A. Kerner, L. Zhao, N. L. Tran, K. M. Lee, T.-W. Koh, G. D. Scholes and B. P. Rand, *Nat. Photonics*, 2017, **11**, 108–115.
10 J. P. Correa Baena, L. Steier, W. Tress, M. Saliba, S. Neutzner, T. Matsui, F. Giordano, T. J. Jacobsson, A. R. Srimath Kandada, S. M. Zakeeruddin, A. Petrozza, A. Abate, M. K. Nazeeruddin, M. Gratzel and A. Hagfeldt, *Energy Environ. Sci.*, 2015, **8**, 2928–2934.
11 S. Yang, W. Fu, Z. Zhang, H. Chen and C.-Z. Li, *J. Mater. Chem. A*, 2017, **5**, 11462–11482.
12 Z. Zhou, S. Pang, Z. Liu, H. Xu and G. Cui, *J. Mater. Chem. A*, 2015, **3**, 19205–19217.
13 H. S. Jung and N.-G. Park, *Small*, 2015, **11**, 10–25.
14 M. A. Green, A. Ho-Baillie and H. J. Snaith, *Nat. Photonics*, 2014, **8**, 506–514.
15 H. Cho, S.-H. Jeong, M.-H. Park, Y.-H. Kim, C. Wolf, C.-L. Lee, J. H. Heo, A. Sadhanala, N. Myoung, S. Yoo, S. H. Im, R. H. Friend and T.-W. Lee, *Science*, 2015, **350**, 1222–1225.
16 Y. Ling, Y. Tian, X. Wang, J. C. Wang, J. M. Knox, F. Perez-Orive, Y. Du, L. Tan, K. Hanson, B. Ma and H. Gao, *Adv. Mater.*, 2016, **28**, 8983–8989.
17 J. C. Yu, A.-Y. Lee, D. B. Kim, E. D. Jung, D. W. Kim and M. H. Song, *Adv. Mater. Technol.*, 2017, 1700003, DOI: 10.1002/admt.201700003.
18 A. B. Chwang, R. C. Kwong and J. J. Brown, *Appl. Phys. Lett.*, 2002, **80**, 725–727.
19 N. C. Erickson and R. J. Holmes, *Appl. Phys. Lett.*, 2010, **97**, 083308.
20 Y.-H. Kim, H. Cho, J. H. Heo, T.-S. Kim, N. Myoung, C.-L. Lee, S. H. Im and T.-W. Lee, *Adv. Mater.*, 2015, **27**, 1248–1254.
21 D. Belaineh, J.-K. Tan, R.-Q. Png, P.-F. Dee, Y.-M. Lee, B.-N. N. Thi, N.-S. Ridzuan and P. K. H. Ho, *Adv. Funct. Mater.*, 2015, **25**, 5504–5511.
22 Y. Wu, X. Yang, W. Chen, Y. Yue, M. Cai, F. Xie, E. Bi, A. Islam and L. Han, *Nat. Energy*, 2016, **1**, 16148.
23 A. Rajagopal, P.-W. Liang, C.-C. Chueh, Z. Yang and A. K. Y. Jen, *ACS Energy Lett.*, 2017, **2**, 2531–2539.
24 Y. Liu, L. A. Renna, M. Bag, Z. A. Page, P. Kim, J. Choi, T. Emrick, D. Venkataraman and T. P. Russell, *ACS Appl. Mater. Interfaces*, 2016, **8**, 7070–7076.
25 H. Zhang, J. Shi, L. Zhu, Y. Luo, D. Li, H. Wu and Q. Meng, *Nano Energy*, 2017, **43**, 383–392.
26 Y.-K. Chih, J.-C. Wang, R.-T. Yang, C.-C. Liu, Y.-C. Chang, Y.-S. Fu, W.-C. Lai, P. Chen, T.-C. Wen, Y.-C. Huang, C.-S. Tsao and T.-F. Guo, *Adv. Mater.*, 2016, **28**, 8687–8694.
27 Q. Chen, N. De Marco, Y. Yang, T.-B. Song, C.-C. Chen, H. Zhao, Z. Hong, H. Zhou and Y. Yang, *Nano Today*, 2015, **10**, 355–396.
28 W. Peng, L. Wang, B. Murali, K.-T. Ho, A. Bera, N. Cho, C.-F. Kang, V. M. Burlakov, J. Pan, L. Sinatra, C. Ma, W. Xu, D. Shi, E. Alarousu, A. Goriely, J.-H. He, O. F. Mohammed, T. Wu and O. M. Bakr, *Adv. Mater.*, 2016, **28**, 3383–3390.
29 A. Kumar, N. K. Kumawat, P. Maheshwari and D. Kabra, 2015.
30 R. J. Elliott, *Phys. Rev.*, 1957, **108**, 1384–1389.
31 M. I. Dar, G. Jacopin, S. Meloni, A. Mattoni, N. Arora, A. Boziki, S. M. Zakeeruddin, U. Rothlisberger and M. Grätzel, *Sci. Adv.*, 2016, **2**, e1601156.
32 Y. Shao, Z. Xiao, C. Bi, Y. Yuan and J. Huang, *Nat. Commun.*, 2014, **5**, 5784.
33 D. M. Jang, K. Park, D. H. Kim, J. Park, F. Shojaei, H. S. Kang, J.-P. Ahn, J. W. Lee and J. K. Song, *Nano Lett.*, 2015, **15**, 5191–5199.
34 J. Emara, T. Schnier, N. Pourdavoud, T. Riedl, K. Meerholz and S. Olthof, *Adv. Mater.*, 2016, **28**, 553–559.
35 Y. F. Ng, N. F. Jamaludin, N. Yantara, M. Li, V. K. R. Irukuvarjula, H. V. Demir, T. C. Sum, S. Mhaisalkar and N. Mathews, *ACS Omega*, 2017, **2**, 2757–2764.
36 J. Wang, N. Wang, Y. Jin, J. Si, Z.-K. Tan, H. Du, L. Cheng, X. Dai, S. Bai, H. He, Z. Ye, M. L. Lai, R. H. Friend and W. Huang, *Adv. Mater.*, 2015, **27**, 2311–2316.
37 R. Meerheim, M. Furno, S. Hofmann, B. Lüssem and K. Leo, *Appl. Phys. Lett.*, 2010, **97**, 253305.
38 S. S. Lim, W. K. Chong, A. Solanki, H. A. Dewi, S. Mhaisalkar, N. Mathews and T. C. Sum, *Phys. Chem. Chem. Phys.*, 2016, **18**, 27119–27123.
39 M. Saba, M. Cadelano, D. Marongiu, F. Chen, V. Sarritzu, N. Sestu, C. Figus, M. Aresti, R. Piras, A. Geddo Lehmann, C. Cannas, A. Musinu, F. Quochi, A. Mura and G. Bongiovanni, *Nat. Commun.*, 2014, **5**, 5049.
40 N. K. Noel, A. Abate, S. D. Stranks, E. S. Parrott, V. M. Burlakov, A. Goriely and H. J. Snaith, *ACS Nano*, 2014, **8**, 9815–9821.
41 C. Hilsum, *Electron. Lett.*, 1974, **10**, 259–260.
42 J.-H. Jou, S. Kumar, A. Agrawal, T.-H. Li and S. Sahoo, *J. Mater. Chem. C*, 2015, **3**, 2974–3002.
43 Y. Kawabe and J. Abe, *Appl. Phys. Lett.*, 2002, **81**, 493–495.
44 A. P. Kulkarni, C. J. Tonzola, A. Babel and S. A. Jenekhe, *Chem. Mater.*, 2004, **16**, 4556–4573.